Effect of film thickness on the structural, electrical and optical properties of sol-gel derived scandium doped zinc oxide films

Ruchika (Sharma) Joshi[1], R. M. Mehra[2, *] and Ajay Kumar[3]

[1]*Department of Physics, Deshbandhu College (University of Delhi), Kalkaji, New Delhi-110019, India.*

[2]*Professor Emeritus, School of Engineering and Technology, Sharda University, Greater Noida-201306, India.*

[3]*Department of Physics, Dharma Samaj College (Dr. B. R. A. University, Agra), Aligarh, India-202001,*

We report the structural, electrical and optical properties of scandium doped zinc oxide (ZnO:Sc) thin films prepared by sol-gel technique and deposited on Corning (7059) glass substrates. The characteristics electrical and optical properties of the prepared ZnO:Sc films are found to strongly depend on both, the doping concentration (of scandium) and the thickness of the film. On increasing the film thickness, the improvement in the c-axis orientation and increase in the grain size has been observed and confirmed by increased intensity of the (0 0 2) peak and the decreased FWHM of the peak. The electrical resistivity of ZnO:Sc films has been decreased considerably (from 1.23×10^{-2} to 3.52×10^{-4} Ω-cm) on increasing the film thickness from 89 to 456 nm. In the visible region, the figure of merit was observed higher for 456 nm thick ZnO:Sc film which may be attributed to the low sheet resistance (771 Ω / square) and high average visible transmission ~ 94%. The surface morphology of the film up to the thickness 349 nm indicated the formation of nanorods.

Keywords- Zinc oxide, Scandium, Sol–gel technique film thickness, electrical and optical properties of thin films

*** Corresponding author,**

Ruchika (Sharma) Joshi

Highlight:

- Significant thickness dependent structural, electrical and optical properties of scandium doped zinc oxide thin films have been observed.
- The electrical resistivity of Sc doped ZnO films is found to decrease (from 1.23×10^{-2} to 3.52×10^{-4} Ω-cm) with increase in thickness from 89 to 456 nm.
- The experimental outcomes based on electrical resistivity, optical transmittance and Hall mobility measurements indicated that the Sc doped ZnO films with 416 nm thickness exhibit optimal characteristics.

1. Introduction

The excellent features such as its abundance in nature, relatively low cost, easy fabrication, low electrical resistivity, non-toxicity, good optical transparency (in the visible region), direct energy band gap, high chemical and mechanic stability *etc.*, have been the key characteristics that attracted the researchers to utilize zinc oxide (ZnO) in variety of applications [1] [2] [3] [4]. ZnO, in the form of its thin films, has been extensively utilized in optoelectronic, photovoltaic, and piezoelectric devices [4]. Various investigations on the electro-optical properties have revealed ZnO thin films as a potential candidate to be used as transparent conducting material (having significant chemical and mechanical stability) in electronic and display devices [5] [6] [7] [8]. The tunable electrical and optical properties have further extended the utility of ZnO thin films in photo sensors, photodetectors, light-emitting diodes, gas sensors, varistors thin film solar cells, liquid crystal displays [9] [10] [11] [12]. Due to the lack of stoichiometry ZnO is generally a wide-gap semiconductor resulting mainly from oxygen vacancies [13].]. Such vacancies cause the formation of deep trap levels in the energy band [14]. To effectively tailor the physical and chemical characteristics such as crystallographic, morphological, optical, electrical, and magnetic etc., the researchers have been doping ZnO with M^{+3} elements (M = Sc, In, Ga, Y, Al, B, Tl) [15] [16]. In a recent report, experimental investigations exploring the effect of concentration, aging, and annealing time on the optical and structural properties of pure and Al doped ZnO thin films have been presented [17]. The modification in the characteristic properties is known to depend strongly on differences in the ionic radii of host ZnO and the impurity atoms [18]. The doping of yttrium, boron, gallium, indium, aluminum, and thallium etc., may introduce lattice strain because of difference in their radius (Y^{3+} =0.0900 nm, B^{3+} =0.0970 nm, In^{3+} =0.0800 nm, Al^{3+}

= 0.0535 nm, Ga^{3+} =0.0620 nm, Tl^{3+} = 0.0885 nm and Zn^{2+} =0.0740 nm) [19] [20] [21] [22] [23]. Among the discussed doping impurities, the scandium possesses the comparable ionic radius to that of host zinc atom (Sc^{3+} =0.0745 nm, and hence Sc could be a suitable doping element for ZnO to observe improved properties of the ZnO:Sc structure [19] [21] [22] [23]. As Sc^{3+} ion exactly fits in the size of Zn^{2+}, the conductivity of epitaxial Sc-doped ZnO thin films is dominated by a degenerated interface layer with pronounced Sc accumulation in the concentration depth profile and hence, scandium could be doped with higher concentrations without causing any remarkable lattice strain in the resulting ZnO:Sc structure [23]. The substation/placement of Sc^{3+} ions at Zn^{2+} lattice sites or on interstitial lattice positions in ZnO:Sc films could bring about an improvement in electrical and optical characteristics of ZnO. Moreover, the electrical conductivity of ZnO thin films has further been modified either by non-stoichiometry of pure ZnO films or by doping a suitable impurity [24] [25] [26] [27] [28] [29]. Although, the ionic radius of Sc^{3+} (0.0745 nm) is very close to that of Zn^{2+} (0.0740 nm), the investigations on Sc doped ZnO thin films have rarely been reported. In 2000, Minami *et al.* first reported Sc and Y doped ZnO films prepared by DC magnetron sputtering using a target made up of a mixture of ZnO and Sc_2O_3 (or ZnO and Y_2O_3) powder [15]. C.-Xing *et al.*, have used RF magnetron sputtering to grow Sc doped ZnO films [30]. They varied the annealing temperature from 250-300^{0}C and observed optical transparency > 90% in 400-800 nm regime. In a couple of studies, Sharma *et al.*, have deposited ZnO:Sc films (derived by using sol-gel technique) on the corning (7059) glass substrates and investigated their structural, electrical and optical properties [31] [5]. The authors varied the doping concentration of scandium as well as the annealing temperature and observed 0.5 wt.% Sc doping (annealing temp. 400^{0}C) as the optimal concentration to achieve stable and better

properties of ZnO:Sc films. The resistivities of the ZnO:Sc thin films were observed lower than that of ZnO:Y thin films; the lowest resistivity (3.1×10^{-4} V cm) was obtained in the ZnO:Sc thin films for Sc_2O_3 content of 2 wt.%. by Mehra *et al.* [32] [33]. Lin *et al.,* [34-36] reported Al–Sc co-doped ZnO films by RF- and DC-sputtering of the ZnO and Al–xSc targets, respectively. Yumak *et al.*, have obtained Sc doped ZnO films using sol-gel technique by varying the dopant concentration from 1 to 7 wt. % [37]. The authors showed 1 wt.% Sc doping as the optimal value to observe strong hybridization of Sc and O atoms. Recently, Bosak et al, have used high frequency pulse-periodic laser action to grow Sc doped (0.9 wt. %) ZnO films and have investigated the electro-physical properties. They proposed that the main conduction mechanism in such films is current limited by space charge with deep trap.

The thickness of the deposited layer could play a crucial role in determine the crystalline quality, preferred orientation and hence the electrical and optical properties of the grown films. So, it becomes essential to investigate the effect of the film thickness on the structural, electrical and optical properties of pure as well as Sc doped ZnO thin films. In this paper, we have presented the experimental results based on pure and scandium doped ZnO (ZnO:Sc) films deposited using spin coating technique of sol–gel process and demonstrated the thickness dependence of the structural and electrical properties of Sc doped ZnO films.

2. Materials and Methods

2.1 Preparation of pure and scandium doped (ZnO:Sc) films

Sol–gel technique offers many advantages for the fabrication of coatings, including excellent control of the stoichiometry of precursor solutions, ease of compositional modifications, customizable microstructure, relatively low annealing temperatures, the possibility of coating

deposition on large-area substrates, and inexpensive equipment. Sol–gel preparations are therefore ideal for exploratory studies for a large number of materials, compositions or preparatory conditions that require screening. So, in present study, we have used sol-gel technique to obtain pure and Sc doped ZnO films. For that, the precursor solution was prepared from zinc acetate dihydrate [Zn $(CH_3COO)_2 \bullet 2H_2O$] (99.95%), (GR, Hayashi Pure Chemical Ind. Ltd, Japan), anhydrous 2-methoxyethanol (AR, Ajax Chemicals, Australia) and monoethanolamine [MEA] (CP, Bio-Lab, London). The solution containing MEA/Zn with molar ratio of 0.2 was stirred for 5 min. An appropriate amount (0–1.5wt %) of scandium nitrate hexahydrate [$(ScNO_3.6H_2O)$, purity 99.9%] was introduced as a dopant. This mixture was sonicated for about two hours. The resultant clear, transparent and homogenous solution was used after 48 hours for film deposition. Microscopic corning glass (7059) slide substrates were cleaned ultrasonically, first in acetone and then subsequently in methanol for ten minutes each. They were further cleaned with deionized water for 20 minutes and finally dried in the nitrogen atmosphere. The spinning speed and time were optimized to 3200 rpm and 30s to ensure that each spun layer is thin enough to ensure the simultaneous evaporation of all solvent, thus preventing the cracking of the films. The wet films were kept to hydrolyze in air at room temperature for 5 minutes, then dried at 200 °C for next 10 minutes and finally heated at 280 °C for 20 minutes in the air atmosphere with a heating rate of about 10 °C/min. Thus, the drying process removed the residual organic solvents and organic groups in the deposited gel film and converted the organic precursor film into a dense inorganic film. An approximate thickness of 0.02 µm was obtained for each spin. The above process of coating and drying was repeated several times to increase the film thickness. In the present work, the thickness of the films was in the range of 450-500 nm. Finally, the deposited films were

annealed in air in the temperature range of 300–500 °C for 1 hr. A slow cooling rate was maintained to avoid the possibility of stress in the films as expected in rapid cooling.

2.2 Characterization of pure and scandium doped ZnO films

Crystallite phase and orientation were evaluated by the X-ray diffraction method (XRD, Philips PW 1830 Geiger counter diffractometer, PW 1830) using a monochromatized X-ray beam with nickel-filtered Cukα radiation (λ= 1.5418 Å). A continuous scan mode was used to collect 2(θ) data from 30 to 40 degrees, with a 0.02 sample pitch and 4 deg/min scan rate. Microstructure was investigated by the scanning electron microscope (SEM, JEOL JSM-6300). Average surface roughness of the films was obtained by an atomic force microscope (AFM, Burleigh- SPI 3700) with a scanned area of 5×5 μm. The thickness of the films was determined by DEKTECK3-ST surface profilometer. Optical transmittance was obtained in the wavelength range of 200-800 nm using the Shimadzu UV-3150 spectro-photometer. The electrical resistivity (ρ) and the Hall coefficient (R_H) were measured by the van der Pauw technique [38]. The sign of the Hall coefficient confirmed the n-type conduction of the films. The composition of scandium doped ZnO films was determined by the Elemental Dispersion Analysis using X-rays (EDAX) measurements.

3. Results and discussion

The pure as well as Sc doped ZnO films grown on Corning glass substrates were first characterized for their structural properties using technique and then, the measurements for electrical resistivity and optical transmission have been carried out. We have discussed these results for pure ZnO films followed by Sc doped ZnO films.

3.1 X-ray diffraction studies of pure ZnO films

The pure ZnO films of different thicknesses were deposited on corning glass (7059) slide substrates using controlled spin coating. The variation in the film thickness was observed almost proportional to the number of deposition cycles performed [Figure 1 (a)]. The linear variation of film thickness with the number of cycles is representing a typical characteristic of the sol-gel technique. Figure 2 (b) shows the X-ray diffractograms of ZnO films of different thickness annealed at 400^{o}C. A single peak corresponding to the c-axis orientation (002) of very weak intensity was observed for the thinnest film (92 nm) [Fig. 2 (b). For the film of thickness 163 nm, two other orientations corresponding to (101) and (100) were appeared along with the (002) peak. On further increasing the thickness up to 642 nm, the intensity as well as sharpness of (002) peak has been increased with the thickness of the film. This indicates that the crystalline quality of the films improved on increasing the thickness of the films.

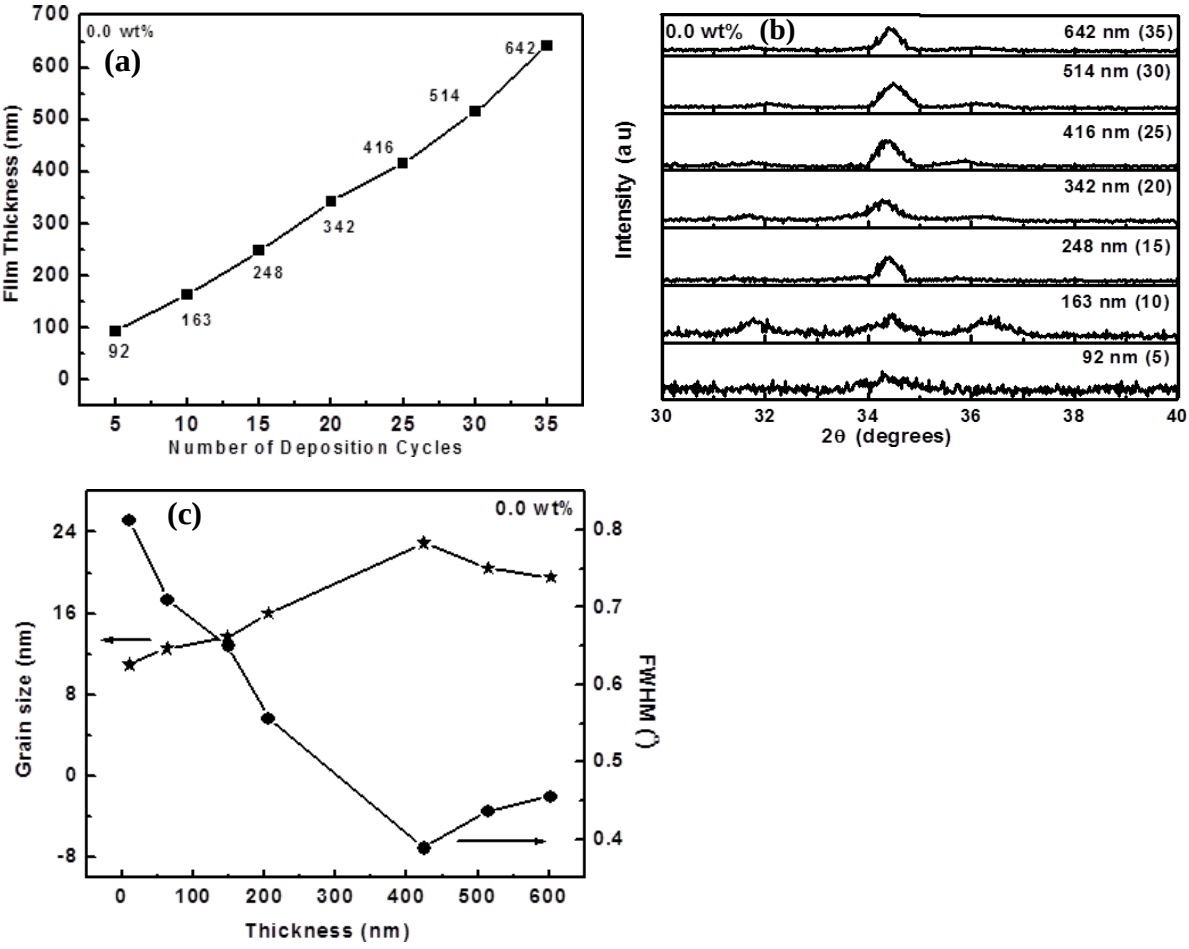

Figure 1: (a) Thickness of ZnO films as a function of number of deposition cycles, (b) X-ray diffractograms of ZnO films with varying thickness annealed at 400◦C, and (c) Variation of film thickness on grain size and full width at half maximum (FWHM) of ZnO film.

The grain size of the films, initially, increased with film thickness (up to 416 nm) and get almost saturated for more thicker films [Figure 2 (c)]. As the film thickness is increased, the value of FWHM is decreased till its minimum at ~0.22 ^{o} for film of thickness 416 nm [Figure 2 (c)]. On further increasing the film thickness, the intensity of (002) peak did not show a significant change whereas the FWHM showed a slight increase. The grain size as determined

from the value of FWHM using Scherer's relation [15] is found to increase from 9 to 26 nm with an increase in film thickness.

As the sample thickness increased from 92 nm to 342 nm, the width of (002) peak narrows, and its position has shifted to a higher 2Θ angle; closer to the corresponding (002) peak position of powder standard (*i.e.*, 34.44 in 2Θ). This shift of larger angle indicated that the 'd' spacing of the (002) plane is decreasing, suggesting that thinner films contain residual compressive macro strain. The decrease in the intensity of (002) peak with the increase in thickness more than 416 nm, may be due to the degradation of film quality. This degradation may be due to the loose structure of the films results in the FWHM and grain size changed their behavior after 416 nm. It may be concluded from figure 2 that the film of thickness 416 nm exhibited the better intensity and FWHM values.

3.2 Optical properties of pure ZnO films

Transmittance measurements were carried out in the 300-800 nm range of spectrum to study the effect of film thickness on the optical properties such as transmittance and band gap of pure ZnO films [Figure 3]. The films of different thicknesses showed higher and constant optical transparency (>84%), along with the interference fringe pattern, throughout the entire visible range. However, the ZnO film of 416 nm exhibited the maximum transmittance (~94%) for 416 nm thick film and the minimum transmittance was observed to be ~85% for 642 nm thick film. The average transmittance remains constant for all the samples for the whole range of spectra recorded.

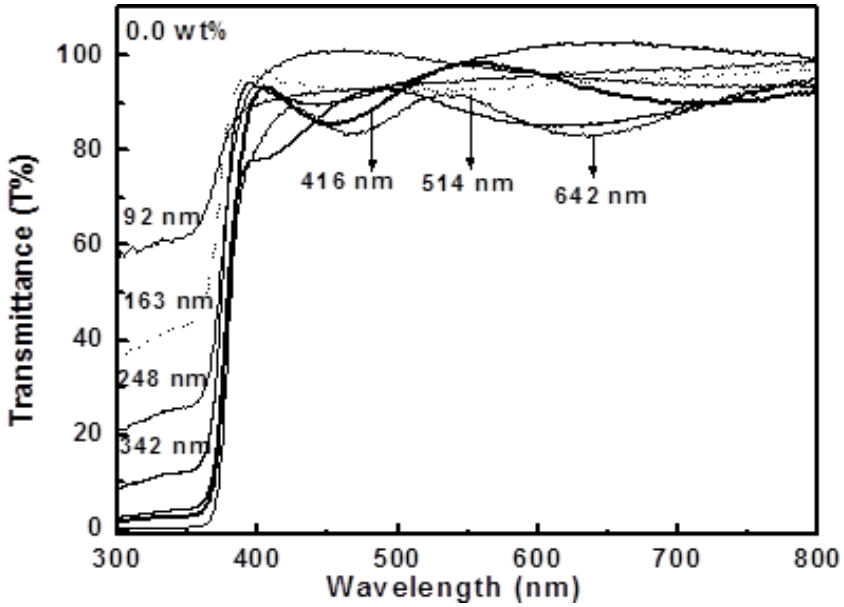

Figure 3: Variation of percent transmission as a function of film thickness for ZnO films. The increase in optical transmittance intensity can be understood with the help of the relation;

$$I = I_o e^{-\alpha d}$$

where I, is the intensity of transmitted light, I_o is the intensity of incident light and d is the thickness of film. The optical absorption co-efficient 'α' is measured as

$$\alpha = \frac{1}{d} \ln \frac{100}{T}$$

where T is the transmittance which is also related to reflection as given in the equation below

$$T = (1 - R)^2 e^{-\alpha d}$$

where R is the reflectance.

In a direct transition semiconductor, α and optical band gap E_g are given by

$$\alpha h\nu = A\left(h\nu - E_g\right)^{\frac{n}{2}}$$

where h is the Planck's constant and ν is the frequency of incident photon. The photon energy at which α^2 is zero is the band gap 'E_g' and is determined by the extrapolation of α^2 versus hν (Tauc's plot) graph on the x-axis.The dependence of E_g on carrier concentration is analyzed considering the Burstein Moss (BM) model for the absorption edge shift ΔE^{BM} in an n-type semiconductor which is given by

$$\Delta E^{BM} = \left(3\pi^2 N\right)^{2/3} \frac{\hbar^2}{2m^*}$$

where m* is the effective mass of the electron and N is the carrier concentration. Shift of the optical absorption edge has been observed on increasing in the film thickness. This feature is commonly observed for highly conducting films and is known as BM shift [39]. In the near-infrared range, thickness affects the transmittance and a sharp decrease in the transmittance is exhibited by all the samples. Figure 4 (a) shows the Tauc's plot for optical band gap as a function of film thickness for the ZnO films. It can be seen from the figure that the band gap of ZnO films was observed to increase from 3.22 to 3.28 eV as the film thickness increased. The increase in Eg with thickness may be attributed to the increase in the grain size and the stress relieving process in ZnO films. The decrease in the transmittance for the films with thicknesses > 416 nm may be due to the degradation in the films' quality caused by the reduction in the adhesion coefficient for source elements arriving at the substrate. So, the decrease in the transmittance may be due to (i) the increase in the film thickness or in the film roughness (ii) the degradation in the films' quality. This is supported by our XRD data as shown in figure 1(b) and (c). The variation of sheet resistance with film thickness of the ZnO films is shown in Figure 4 (b). The sheet resistance is observed to decrease with thickness up

to 416 nm film thickness and, then started slightly increasing [Figure 4 (b)]. The minimum sheet resistance of ~ 1071Ω/□ is obtained for a 416 nm thick ZnO film. The average optical transmittance of the ZnO films was observed to increase with the film thickness since the thickness 416 nm and, it decreased on further increasing the film thickness [Figure 4 (b)]. It is clear that the sheet resistance can be brought down to a desired value by increasing the film thickness but beyond 416 nm, the sheet resistance increases and hence, the 416 nm thick film is found optimal with lowest sheet resistance and good optical transmittance.

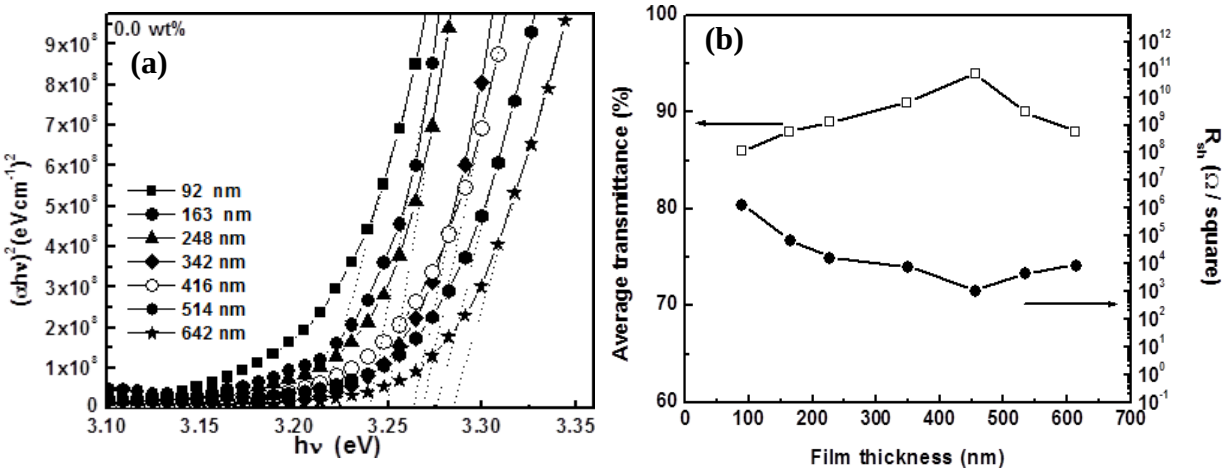

Figure 4: (a) Band gap calculation for ZnO films as a function of film thickness using Tauc's plot, (b) Average Transmittance and Sheet resistance of ZnO films as a function of film thickness

3.3 Electrical properties of undoped ZnO films

Figure 5 shows the behavior of electrical resistivity (ρ), carrier concentration (n) and Hall mobility (μ_H) of pure ZnO films as a function of film thickness. As can be seen, the resistivity of the films was observed to decrease monotonically from ~ 1.2 x 10^{-1} Ω-cm to 3.87 x 10^{-3} Ω-cm as the film thickness increases from 93 nm to 416 nm [Figure 5]. This behavior can be

explained by examining the dependence of carrier concentration and Hall mobility as a function of film thickness. The carrier concentration of the film was steadily increased on increasing the film thickness up to ~ 416 nm. A maximum carrier concentration of 3.2×10^{20} cm^{-3} is measured at this thickness. On further increasing the film thickness, a slight decrease in the carrier concentration was observed. However, noticeable change in resistivity with further increase in film thickness is observed.

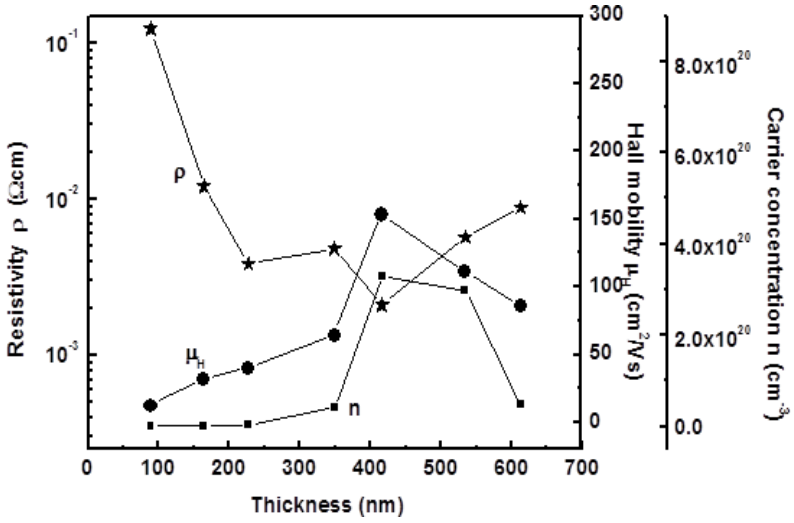

Figure 5: Resistivity (ρ), Carrier concentration (n) and Hall mobility (μ_H) of ZnO films as a function of film thickness.

The Hall mobility of the films was increased initially from 12.76 to 153.7 cm^2/Vs (as the film thickness increases from 89 to 416 nm) and then, it decreased slightly to 86.45 cm^2/Vs, on further increasing the film thickness. The initial increase in the mobility with the film thickness is likely due to the reduction of surface and grain boundary scattering [40]. The decrease in the Hall mobility for films with thickness > 416 nm may be due to the degradation of film quality as seen in the XRD analysis (increased values of FWHM). The lowering of the

mobility has suggested the fact that the surface and grain boundary scattering are no longer dominant scattering mechanisms. Other mechanisms such as ionized impurity scattering could have limited the mobility of the films.

3.4 Characteristics of scandium doped ZnO films

3.4.1 X-ray diffraction studies of scandium doped ZnO films

The XRD patterns of the fabricated thin films have indicated the growth of Sc doped ZnO film to prefer (002) crystalline orientation on plane of zinc oxide polycrystalline with hexagonal würtzite structure [Figure 6]. This (002) crystalline orientation of ZnO:Sc films was earlier observed by Sharma *et al.* [31]. Figure 6 (a) indicates no change in ZnO hexagonal wurtzite structure and no peak of Sc for homogenous scattering scandium atoms in ZnO lattice [10]. Besides strong (002) peak, the (103) orientation can also be seen in Sc doped ZnO films indicating a polycrystalline nature with preferential orientation along the c- axis. The lowering of the crystalline quality of ZnO films on doping with Sc was observed, too, by Chen *et al.* [21]. It can be seen from figure 6 (b) that the intensity and FWHM values of the (002) orientation have been increased/decreased with the film thickness up to 456 nm. The intensity of (002) peak is found to diminish (with a broadened FWHM) for thicker films. This has clearly indicated the deterioration in crystalline quality of the films of thickness greater than 456 nm.

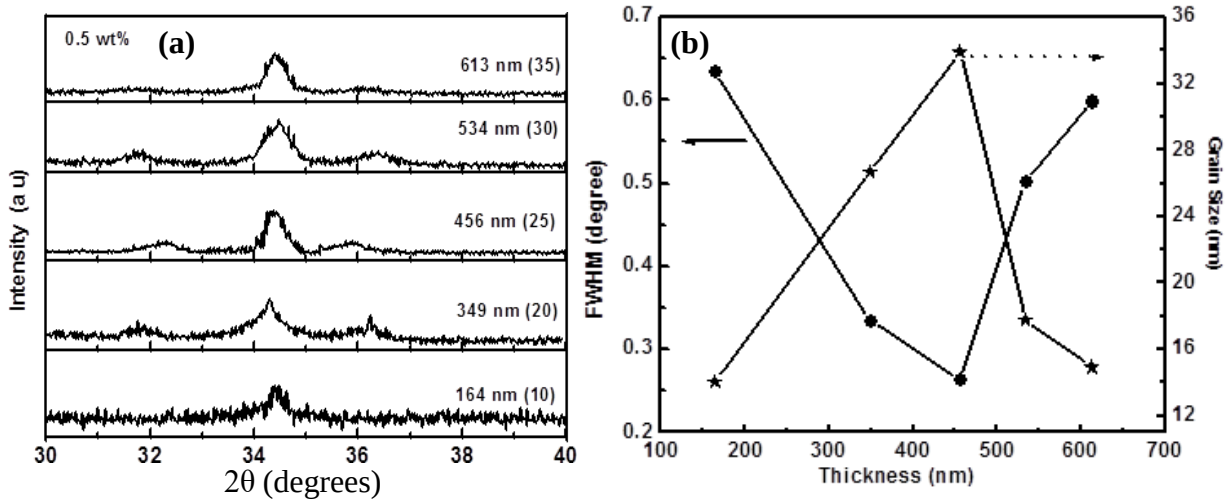

Figure 6: (a) X-ray diffraction patterns for ZnO:Sc films with different thickness and, (b) FWHM of (002) XRD peak and the grain size for ZnO:Sc films with different thickness

According to the kinetics of crystal growth [41], the growing faces of a crystal are part of the free surface of the film. These crystal faces correspond to the crystal shape at equilibrium and are determined by the orientation of the crystal. A growth competition can start among the neighboring crystals according to their growth types (*i.e.*, to their orientation). The faster growing crystals will grow over the slower growing ones. This competition is terminated when only crystals exhibiting the same type of crystal faces proceed to the free surface. This competitive crystal growth represents an orientation selection among the crystals resulting in the competitive growth texture. This was probably why the crystallinity was increased when ZnO:Sc film was thicker. The grain size of ZnO:Sc films with different thickness were calculated using Scherrer's formula [42] [43]. As depicted in figure 6 (b), the grain size increased with increase in the film thickness up to 456 nm and then decreased. Also, the value

of FWHM is decreased with thickness up to 456 nm and then showed an increase in conformity with the variation of grain size.

3.4.2 Surface morphology of Sc doped ZnO films

The effect of Sc doping in ZnO on the morphological appearance was analyzed using scanning electron microscopy (SEM) and atomic force microscopy (AFM) techniques. The planar and cross-sectional SEM micrographs of Sc doped (0.5 wt. %) ZnO films of varying thicknesses is shown in figure 7. Cheng *et al.* [44] demonstrated the synthesis of ZnO colloidal spheres by the sol–gel method. The formation of uniform tightly packed grains can be clearly seen in the micrographs. The size of the grains is found to increase with an increase in thickness of the film. The cross-sectional image clearly indicated a columnar growth of the grains perpendicular to the surface of the substrate. It can be seen that, for the film thicknesses of 349 nm and above, it took place the formation of nanorods. Also, the height of the nanorods is increased and the tip of the rods became dominant at 456 nm thickness. However, on further increasing the thickness, the textures indicated the disappearance of nanorods with clear grain boundaries. As the thickness is further increased to 613 nm, the nanorods have disappeared and junk of wires appears, hinting at degradation of film surfaces. We found that the optimum ZnO:Sc layer thickness condition of 456 nm, the Zn^{+2} can effectively decrease the probability of bimolecular recombination either at the Sc^{+3} interface or within the active layer itself. [46]. It is worth to mention here that the SEM analysis has, too, showed better morphology for the films of thickness 456 nm.

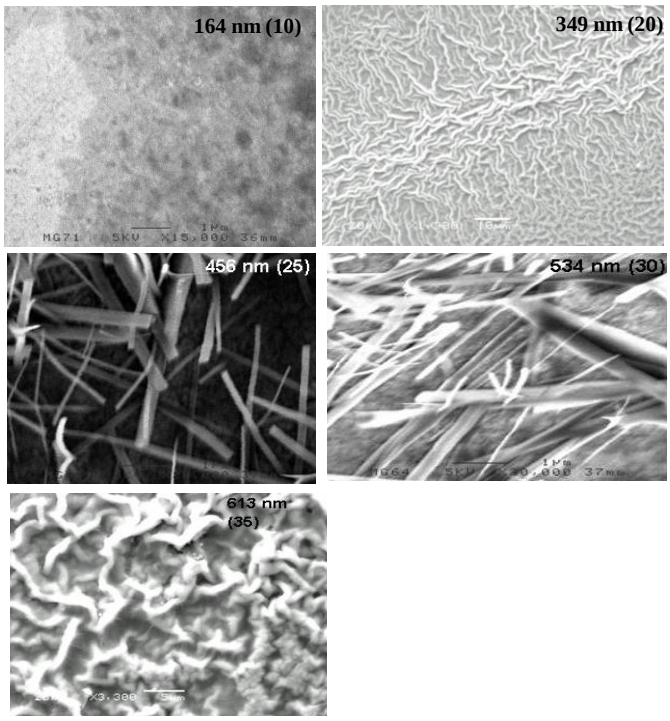

Figure 7: SEM images of Sc doped ZnO films of different thicknesses (164 nm, 349 nm, 456 nm, 534 nm, and 613 nm).

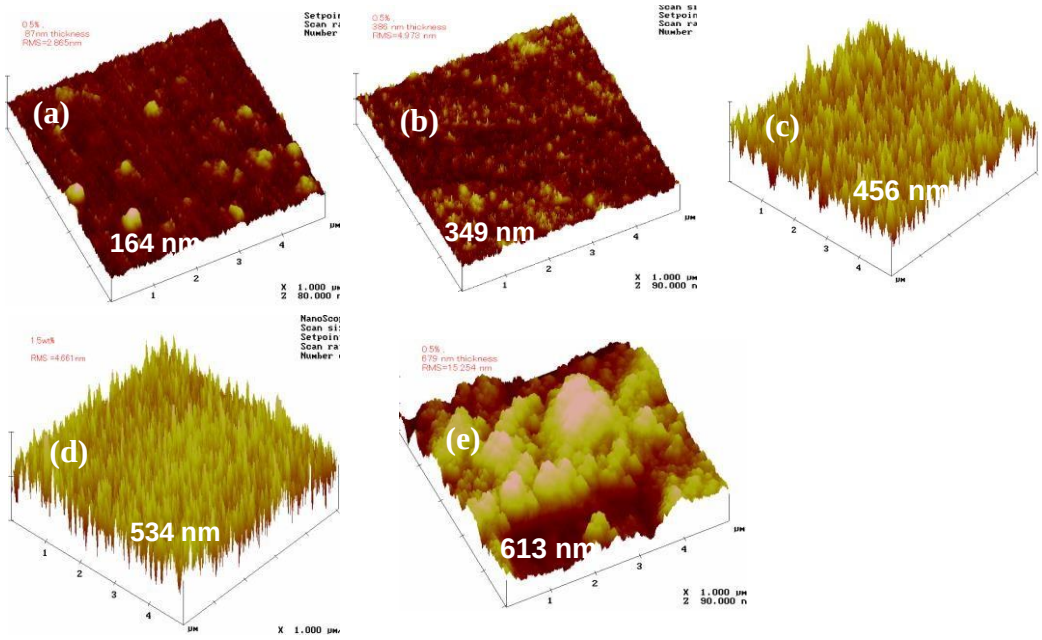

Figure 8: The 3D AFM images of Sc doped ZnO films of different thicknesses.

Figure 8 (a-e) shows the 3D AFM images of Sc doped ZnO films (0.5 wt% and annealed at 400◦C) of varying thicknesses. It can be seen easily from the AFM images that the grown films consist of homogeneous distribution of nanosized particles on the surface of the film. The AFM images indicated that the sizes of nanoparticles have initially increased with the film thickness from 164 nm to 456 nm and then it decreased for thicker films. This could happen due to the increased surface roughness of the films having thickness > 456 nm.

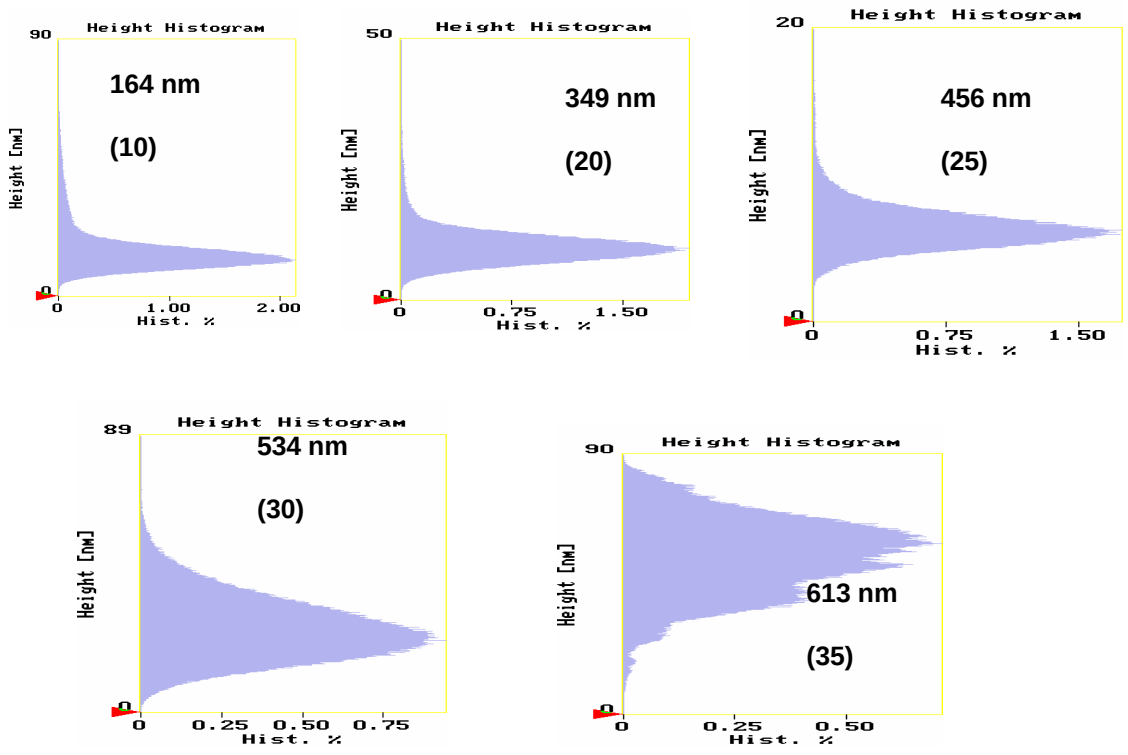

Figure 9: The variation in crystal size with thickness of Sc doped ZnO films as obtained by AFM measurements.

Figure 9 shows the variation in the crystal size with the thickness of the films. As can be seen from the figure that the variation in the crystal size is supportive to the results obtained by

AFM analysis. Clearly, the films of thickness 456 nm are found to have better morphology with biggest grain size.

3.4.3 Optical properties of Sc doped ZnO films

Figure 10 shows the variation of transmittance measurements and Tauc's plot for varying thickness of 0.5 wt. % Sc doped ZnO films recorded in the 300– 800 nm range of spectrum. As can be seen from the figure, the films exhibited higher values of optical transmission (≥84%) with interference fringe pattern in the visible region. The optical transmission was, however, decreased substantially at short wavelengths near the ultraviolet range for all the films. It is worth to notice that the film of thickness 456 nm showed maximum transmission >90% in the visible region.

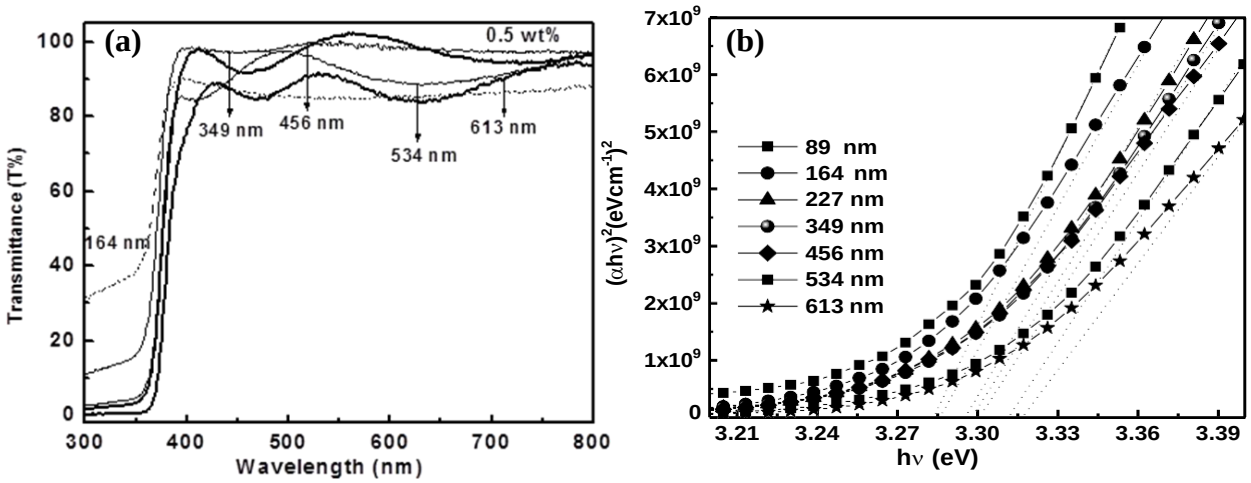

Figure 10: (a) Variation of T % as a function of film thickness and (b)Tauc's plots of ZnO:Sc films as a function of film thickness.

The spectroscopic data in the UV region has showed a shoulder for thinner films (164-349 nm) [Figure 10 (a)]. This could occur due to the larger surface-to-volume ratio for such films and

larger number of defects resulted in distortion of crystallites. Therefore, the Zn^{+2} with the 'd' electron energy level could be split by the effect of crystal field, resulting in the shoulder at short wavelengths. Figure 10 (b) shows the plot of $(\alpha hv)^2$ vs photon energy (hv) for 0.5 wt. % scandium doped ZnO films annealed at different thicknesses. The band gap has increased from 3.272 ev to 3.31 eV on increasing the film thickness from 64 nm to 613 nm due to the improvement in crystallinity. The absorption edge was observed at a slightly lower wavelength range for thinner ZnO:Sc film due to the variation in grain size [46] and/or carrier concentration [47] [48]. The results of XRD [Figure (6)], too, showed that the thinner ZnO:Sc films (164-349 nm) contained relatively small grain size and due to the same, the blue shift has occurred.

Table 1: The sheet resistance, average visible transmission and figure of merit of scandium doped ZnO films with different thickness.

ZnO:Sc film Thickness (nm)	**Transmission T (Visible region)**	**Sheet resistance R_{sh} (Ω /square)**	**Figure of merit Ø ($Ω^{-1}$) (λ = 300–800 nm)**
164	0.881	737×10^{2}	119×10^{-7}
349	0.913	810.8×10	1126×10^{-7}
456	0.946	771	1226×10^{-6}
534	0.904	107.1×10	844×10^{-6}
613	0.882	46×10^{2}	1917×10^{-7}

Table 1 summarizes the figure of merit vs. deposition thickness for the ZnO:Sc films. A figure of merit (Ø = T^{10}/Rsh, where T is the optical transmittance and R_{sh} is the sheet resistance) was defined by Haacke *et al.* [49] and it provides a criterion for the performance of a film. In the visible region, the figure of merit was higher for 456 nm film than the others. It is because the ZnO:Sc films with 456 nm in thickness simultaneously had low sheet resistance (771 Ω / square) and high average visible transmission ~ 94% [Fig 10 (a) and (b)].

3.4.4 Electrical properties of scandium doped ZnO films

The influence of film thickness on resistivity (ρ), carrier concentration (n) and Hall mobility (μ_H) of ZnO:Sc films is shown in figure 11. It is observed that, when the film thickness is less than 164 nm, resistivity is $>10^{-3}$ Ω-cm. However, as the film thickness increases, the resistivity has decreased rapidly from ~ 1.23×10^{-2} Ω-cm (at 89 nm thick) to 2.8×10^{-3} Ω-cm (at 349 nm thick). On increasing the thickness further, the resistivity has decreased slowly to the lowest value of ~3.52×10^{-4} Ω-cm. The lowest resistivity was found to be for the film having thickness 456 nm. With further increase in the film thickness up to 613 nm slight increases in the resistivity was observed. Resistivity increases from 5.72 x 10^{-4} Ω-cm (at a thickness of 534 nm) to 2.8 x 10^{-3} Ω-cm (at a thickness of 613 nm). Jeong *et al* [50] reported the increase in the resistivity with increase in film thickness. This behavior can be explained by examining the dependence of carrier concentration and Hall mobility as a function of film thickness. Carrier concentration was increased rapidly with the increase in film thickness up to ~ 456 nm and there after it decreased slowly. A maximum carrier concentration of 3.27×10^{20} cm^{-3} is measured at a film thickness of 456 nm. On further increasing the film thickness the carrier concentration was observed to decrease. The carrier concentration is found to decrease from $3.27\times10^{20}cm^{-3}$ to 4.6 × 10^{19} cm^{-3} with the increase in thickness from 546 nm to 613 nm.

Mobility decreases initially from 132.5 to 40.28 cm^2/Vs (as the film thickness increases from 89 to 456 nm) and it decreases linearly from 31.86 to 12.76 cm^2/Vs with further increase in the film thickness up to 613 nm [51]. Both the mobility and carrier concentration increased with the increase of film thickness up to 456 nm and then decreased. The decrease in the mobility is likely due to the reduction of surface and grain boundary scattering, which decrease with the increase of film thickness. The increase in the resistivity and decrease in carrier concentration and Hall mobility may be due to the degradation of film quality (546 nm to 613 nm). Observance of higher resistivity values for thinner films could be attributed to poor crystallinity of the films (Figure 11). These films consisted of a few atomic layers of disordered atoms [52] as observed from SEM and AFM images [Figure 7 and 8]. Since the atoms in the poorly crystallized area were disordered, there could be a large number of defects due to incomplete atomic bonding. The surface-to-volume ratio was large for the thinner films, and more defects acting as scattering centers in the thinner films. This resulted in the formation of trapping states which are capable of trapping carriers thereby immobilizing them. This has reduced the number of free carriers available for electrical conduction. After trapping the mobile carriers, the traps become electrically charged, creating a potential energy barrier which impedes the motion of carriers from one crystallite to another, thereby reducing their mobility [53]. Not many carriers were probably released from the poor crystallized area [54].

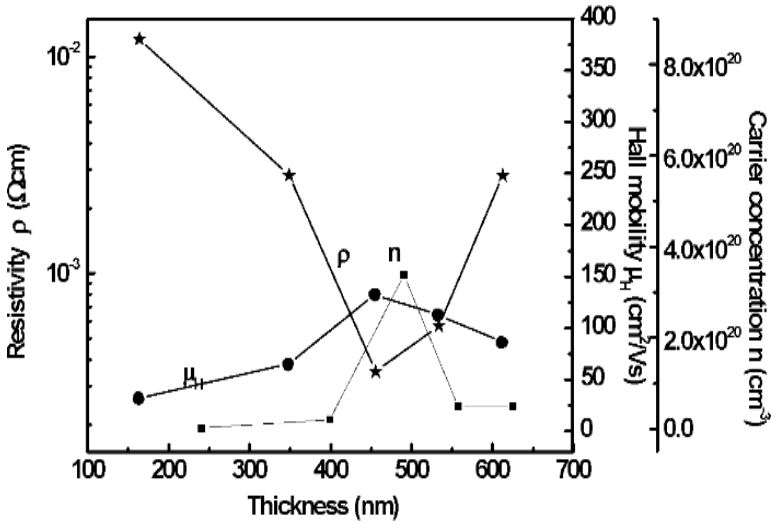

Figure 11: The resistivity (ρ), carrier concentration (n) and Hall mobility (μ_H) as a function of thickness of scandium doped ZnO films.

The poor crystallinity resulted in lower carrier concentration and hence, the conductivity was affected by carrier concentration and mobility in this study. The resistivity ρ is proportional to the reciprocal of the product of carrier concentration n and mobility μ_H [55].

4. Conclusion

High quality transparent and conducting pure and Scandium doped (0.5 wt. %) ZnO films were obtained by spin coating using sol–gel technique. The effect of thickness of the grown films on its structural, electrical and optical properties has been experimentally investigated. The electrical resistivity of Sc doped ZnO films was found to decrease considerably (from 1.23×10^{-2} to 3.52×10^{-4} Ω-cm) on increasing the film thickness from 89 to 456 nm. The figure of merit was found higher for 456 nm thick Sc doped ZnO film in the visible region. It could be attributed to the low sheet resistance (771 Ω / square) and high average visible transmission ~ 94%. It has been found that characteristics of the films is highly dependent on

its thickness and, the film of thickness 456 nm was observed to exhibit the better morphology as well as electrical properties. Such films would find application as solar cell window material. The ZnO doped with Sc (III) ions considered as a low-cost and environment-friendly antibacterial material with highly synergistic antimicrobial activity. The successful growth of conducting and epitaxial ZnO:Sc films on sapphire without using buffer layer demonstrates the feasibility of utilizing these films for optoelectronic devices applications at low cost and on large area substrate.

Acknowledgements- One of the authors Ruchika (Sharma) Joshi gratefully acknowledges the financial assistance of AIEJ, Japan, during her visit to Toyohashi University of Technology, Toyohashi, Japan. The authors also wish to acknowledge the financial support of Department of Physics Deshbandhu college under the aegis of IQAC and DBT STAR college Scheme.

References

[1] B.N.Pawar, Duk-Ho Ham, R.S.Mane, T.Ganesh, Byung-Won Cho, Sung-Hwan Han, Fluorine-doped zinc oxide transparent and conducting electrode by chemical spray synthesis, Appl. Surf. Sci. 254 (2008) 6294–6297. https://doi.org/10.1016/j.apsusc.2008.02.088

[2] F. Chouikh, Y. Beggah, and M. S. Aida, Optical and electrical properties of Bi doped ZnO thin films deposited by ultrasonic spray pyrolysis, J. Mater. Sci.: Mater. Electron. 22 (2011) 499–505. https://doi.org/10.1007/s10854-010-0167-y

[3] R. R. Biswal, S. Velumani, B. J. Babu, A. Maldonado, S. Tirado-Guerrac L. Castañeda, M.de la L. Olver, Fluorine doped zinc oxide thin films deposited by chemical spray, starting from zinc pentanedionate and hydrofluoric acid: Effect of the aging time of the solution, Mater. Sci. Eng. B 174 (2010) 46-49. https://doi.org/10.1016/j.mseb.2010.03.013

[4] L. Znaidi, Sol–gel-deposited ZnO thin films: A review, Materials science and engineering: B. 174 (2010) 18-30. https://doi.org/10.1016/j.mseb.2010.07.001

[5] R., Sharma, K. Sehrawat, R. M. Mehra, Epitaxial growth of highly transparent and conducting Sc-doped ZnO films on c-plane sapphire by sol–gel process without buffer, Current Applied Physics. 10 (2010) 164-170. https://doi.org/10.1016/j.cap.2009.05.013

[6] Xianfa Jiang, Bin Zhang, Biying Liu, Xiaoning Tang, Lihong Tang, Experimental and theoretical study of visible light driven scandium (III) doped ZnO for antibacterial activity. Current Applied Physics 45 (2019) 19948-19955. https://doi.org/10.1016/j.ceramint.2019.06.252

[7] A. Kudo, H. Yanagi, K. Ueda, H. Hosono, H. Kawazoe and Y. Yano, Fabrication of transparent p–n heterojunction thin film diodes based entirely on oxide semiconductors, Appl. Phys. Lett. 75 (1999) 2851. https://doi.org/10.1063/1.125171

[8] M. K. Jayaraj, A. Antony and M. Ramachandran, Transparent conducting zinc oxide thin film prepared by off-axis rf magnetron sputtering, Bull. Mater. Sci. 25 (2002) 227. https://doi.org/10.1007/BF02711158

[9] M. Jiang, X. Liu, and H.Wang, Conductive and transparent Bi-doped ZnO thin films prepared by rf magnetron sputtering, Surf. Coat. Technol. 203 (2009) 3750–3753. https://doi.org/10.1016/j.surfcoat.2009.06.014

[10] G. Turgut and E. Sonmez, A Study of Pb-Doping Effect on Structural, Optical, and Morphological Properties of ZnO Thin Films Deposited by Sol–Gel Spin Coating, Metall. Mater. Trans. A 45A (2014) 3675–3685. https://doi.org/10.1007/s11661-014-2281-6

[11] B. N. Pawar, D.- H. Ham, R. S. Mane, T. Ganesh, B.-W. Cho, S.-H. Han, Fluorine-doped zinc oxide transparent and conducting electrode by chemical spray synthesis, Appl. Surf. Sci. 254 (2008) 6294–6297. https://doi.org/10.1016/j.apsusc.2008.02.088

[12] E. F. Keskenler, M. Tomakin, S. Doğan, G. Turgut, S. Aydın, S. Duman, B. Gürbulak, Growth and characterization of Ag/n-ZnO/p-Si/Al heterojunction diode by sol–gel spin technique, J. Alloy. Compd. 550 (2013) 129–132. https://doi.org/10.1016/j.jallcom.2012.09.131

[13] Iribarren, P. Fernández, J. Piqueras, Cathodoluminescence characterization of ZnO:Te microstructures obtained with ZnTe and TeO_2 doping precursors. Superlattices Microstruct. 43 (2008) 600–604. https://doi.org/10.1016/j.spmi.2007.06.009

[14] R A. Iribarren, P. Fernández, J. Piqueras, TeO_2-doped ZnO micro and nanostructures grown by the vapour–solid technique, Rev. Cuba. Física. 26 (2009) 42–46. http://www.revistacubanadefisica.org/RCFextradata/OldFiles/2009/vol.26-No.1/RCF-26-1-2009-42.pdf

[15] E. F. Keskenler, S. Doğan, G. Turgut and B. Gürbulak, Evaluation of Structural and Optical Properties of Mn-Doped ZnO Thin Films Synthesized by Sol-Gel Technique, Metall. Mater. Trans. A 43A (2012) 5088–5095. https://doi.org/10.1007/s11661-012-1365-4.

[16] G. Turgut, and E. F. Keskenler, Single and multiple doping effects of silicon–boron and fluorine on ZnO thin films deposited with sol–gel spin coating technique, J. Mater. Sci: Mater. Electron. 25 (2014) 273–285. https://doi.org/10.1007/s10854-013-1583-6.

[17] D. T. Speaks, Effect of concentration, aging, and annealing on sol gel ZnO and Al-doped ZnO thin films, International Journal of Mechanical and Materials Engineering 15 (2020)2. https://doi.org/10.1186/s40712-019-0113-6

[18] E. F.Keskenler, G. Turgut, S. Doğan, Investigation of structural and optical properties of ZnO films co-doped with fluorine and indium, Superlattices Microstruct. 52 (2012) 107–115. https://doi.org/10.1016/j.spmi.2012.04.002

[19] S. A. Nasser, Characterization of boron-doped tin oxide thin films, Thin Solid Films 342 (1999) 47–51. https://doi.org/10.1016/S0040-6090(98)01337-6

[20] Chemistry of the Elements, 2nd ed. Reed Educational and Professional Publishing, Oxford, 1997, 1341. 0750633654_TOC.pdf (cern.ch)

[21] J. Chen, D. Chen, J. He, S. Zhang, and Z. Chen, The microstructure, optical, and electrical properties of sol–gel-derived Sc-doped and Al–Sc co-doped ZnO thin films, Appl. Surf. Sci. 255 (2009) 9413–9419. https://doi.org/10.1016/j.apsusc.2009.07.044

[22] J.-C. Lin, K.-C. Peng, I.-G. Peng, S.-L. Lee, Corrosion behavior of Al, Sc-co-doped ZnO thin films in 3.5% NaCl solution, Thin Solid Films 517 (2009) 4777–4781. https://doi.org/10.1016/j.tsf.2009.03.080

[23] A. V. Singh and R. M. Mehra, p-type conduction in codoped ZnO thin films, J. Appl. Phys. 93 (2003) 396. https://doi.org/10.1063/1.1527210

[24] T. Minami, H. Sato, K. Ohashi, T. Tomofuji, S. Takata, Conduction mechanism of highly conductive and transparent zinc oxide thin films prepared by magnetron sputtering, J. Cryst. Growth 117 (1992) 370-374. https://doi.org/10.1016/0022-0248(92)90778-H

[25] J. F. Chang, W. C. Lin, and M. H.Hon, Effects of post-annealing on the structure and properties of Al-doped zinc oxide films, Appl. Surf. Sci. 183 (2001) 18-25. https://doi.org/10.1016/S0169-4332(01)00541-4

[26] Y. Shimizu, F.-C. Lin, Y. Takao, M. Egashira, Zinc Oxide Varistor Gas Sensors: II, Effect of Chromium(III) Oxide and Yttrium Oxide Additives on the Hydrogen-Sensing Properties, J. Am. Ceram. Soc. 81 (1998) 1633. https://doi.org/10.1111/j.1151-2916.1998.tb02525.x

[27] A. E. Jiménez-González Jose, A. Soto Urueta, R. Suárez-Parra, Optical and electrical characteristics of aluminum-doped ZnO thin films prepared by solgel technique, J. Cryst. Growth 192 (1998) 430-438. https://doi.org/10.1016/S0022-0248(98)00422-9

[28] A. V. Singh and R. M. Mehra, Highly conductive and transparent aluminum-doped zinc oxide thin films prepared by pulsed laser deposition in oxygen ambient, J. Appl. Phys. 90 (2001) 5661. https://doi.org/10.1063/1.1415544

[29] C.-X. Miao, Z.-X. Zhao, Zhao Lei, Ma Z.-Q. Ma, Substrate temperature dependence of the properties of scandium-doped ZnO films deposited by sputtering, Appl. Surface Science. 256 (2010) 3174-3177. https://doi.org/10.1016/j.apsusc.2009.12.001

[30] K. -S. Hwang, S. Hwangbo, J.-T. Kim, The influence of the prefiring temperature on the structure and surface morphology of sol-gel derived ZnO film, Materials Science-Poland, 27 (2009) 159. Microsoft Word - indeks 2009.doc (pwr.edu.pl)

[31] T. Minami, Highly transparent and conductive rare earth-doped ZnO thin films prepared by magnetron sputtering, Thin Solid Films 366 (2000) 63. https://doi:10.1016/S0040-6090(00)00731-8

[32] R. Kaur, A. V. Singh, and R. M. Mehra, Sol–gel derived highly transparent and conducting yttrium doped ZnO films, J. Non-Cryst. Solids 352 (2006) 2335. https://doi.org/10.1016/j.jnoncrysol.2006.03.011

[33] Q.Yu, H.Yang, W. Fu , L. Chang, J. Xu, C.Yu, R.Wei. K. Du, H. Zhu, M. Li G. Zou, Transparent conducting yttrium-doped ZnO thin films deposited by sol–gel method, Thin Solid Films 515 (2007) 3840-3843. https://doi.org/10.1016/j.tsf.2006.10.077

[34] J. Lin, Transparent conducting Sc-codoped AZO film prepared from ZnO:Al Sc by RF-DC sputtering, Thin Solid Films 516 (2008) 5349-5354. https://doi:10.1016/j.tsf.2007.07.096

[35] K.-C. Peng, J.-C. Lin, C. A. Tseng, S.-L. Lee, Characterization of the single and double films consisting of Al, Sc-co-doped ZnO/Al-doped ZnO and Al-doped ZnO/Al, Sc-co-

doped ZnO, Surf. Coat. Technol. 202 (2008) 5425-5430. https://doi.org/10.1016/j.surfcoat.2008.06.089

[36] A.Yumak, G. Turgut, O. Kamoun et al., Stability and morphology-dependence of Sc3+ ions incorporation and substitution kinetics within ZnO host lattice, Materials science in semiconductor processing. 39 (2015)103-111. https://doi.org/10.1016/j.mssp.2015.04.010

[37] N. A. Bosak, A. N. Chumakov, A. A. Shevchenok, L. V. Baran, A. G. Karoza, V. V. Malutina-Bronskaya, T. F. Raichenok and M. G. Sugak, Optical and electrophysical properties of thin zinc oxide films doped with scandium and obtained by laser deposition, J. Appl. Spectroscopy 87 (2020) 840-845. https://doi.org/10.1007/s10812-020-01079-y

[38] E. Burstein, Anomalous Optical Absorption Limit in InSb, Phys. Rev. 93 (1954) 632. https://doi.org/10.1103/PhysRev.93.632

[39] X. Hao, J. Ma, D. Zhang, T.Yang, H. Ma, Y.Yang, C. Cheng, J. Huangd, Thickness dependence of structural, optical and electrical properties of ZnO:Al films prepared on flexible substrates, Appl. Surf. Sci., 183 (2001) 137-142. https://doi.org/10.1016/S0169-4332(01)00582-7

[40] P. B. Barna, M. Adamik, Fundamental structure forming phenomena of polycrystalline films and the structure zone models, Thin Solid Films 317 (1998) 27-33. https://doi.org/10.1016/S0040-6090(97)00503-8

[41] Laurent Sagalowicz, and Glen R. FoxPlanar defects in ZnO thin films deposited on optical fibers and flat substrates, J. Mater. Res. 14 (5) (1999) 1876-1885. https://doi.org/10.1557/JMR.1999.0252

[42] G. Sanon, R. Rup, A. M. Singh, Growth and characterization of tin oxide films prepared by chemical vapour deposition, Thin Solid Films 190 (1990) 287-301. https://doi.org/10.1016/0040-6090(89)90918-8

[43] H.-M. Cheng, H.-C. Hsu, S.-L. Chen, W.-T. Wu, C.-C. Kao, L.-J. Lin, and W.-F. Hsieh, Efficient UV Photoluminescence from Monodispersed Secondary ZnO Colloidal Spheres Synthesized by Sol-Gel Method, J. Cryst. Growth 277 (2005) 192-199. https://doi.org/10.1016/j.jcrysgro.2004.12.133

[44] M. Wang, Y. Li, et al, Thickness dependence of the MoO3 blocking layers on ZnO nanorod-inverted organic photovoltaic devices.Appl. Phys. Lett. 98 (2011) 103305. https://dx.doi.org/10.1063%2F1.3554381

[45] The Materials Science of Thin Films, Academic Press, San Diego, CA, 1991, p. 379.

[46] W. Tang D. C.Cameron, Aluminum-doped zinc oxide transparent conductors deposited by the sol-gel process, Thin Solid Films 238 (1994) 83-87. https://doi.org/10.1016/0040-6090(94)90653-X

[47] B. E. Sernelius, K.-F. Berggren, Z.-C. Jin, I. Hamberg, and C. G. Granqvist, Band-gap tailoring of ZnO by means of heavy Al doping, Phys. Rev., B 37 (1988) 10244. https://doi.org/10.1103/PhysRevB.37.10244

[48] S. Redfern, (1993). A. Putnis (1992). Introduction to Mineral Sciences. xxii 457 pp. Cambridge, New York, Port Chester, Melbourne, Sydney: Cambridge University Press. https://doi.org/10.1017/S0016756800009948

[49] G. Haacke, New figure of merit for transparent conductors, J. Appl. Phys. 47 (1976) 4086. https://doi.org/10.1063/1.323240

[50] W-Jo Jeong and G-Choon Park, Sol. Ene. Mat. & Sol. Cells., 65 (2001) 37. DOI:10.1021/ma102080c

[51] L. L. Kazmerski, W. B. Berry and C. W. Allen, Role of defects in determining the electrical properties of CdS thin films. I. Grain boundaries and surfaces, J. Appl. Phys., 43 (1972) 3515. https://doi.org/10.1063/1.1661746

[52] John Y. W. Seto, The electrical properties of polycrystalline silicon films, J. Appl. Phys. 46 (12) (1975) 5247. https://doi.org/10.1063/1.321593

[53] P. Rai-Choudhury and P. L. Hower, Growth and Characterization of Polycrystalline Silicon, J. Electrochem. Soc. 120 (1973) 1761. https://doi.org/10.1149/1.2403359

[54] T. I. Kamins, Hall Mobility in Chemically Deposited Polycrystalline Silicon, J. Appl. Phys. 42 (1971) 4357. https://doi.org/10.1063/1.1659780

[55] H. Morikawa, M. Fujita, Crystallization and decrease in resistivity on heat treatment of amorphous indium tin oxide thin films prepared by d.c. magnetron sputtering, Thin Solid Films 339 (1999) 309-313. https://doi.org/10.1016/S0040-6090(98)01156-0